

User Selection in Near-Field Gigantic MIMO Systems with Modular Arrays

José P. González-Coma, Santiago Fernández, and F. Javier López-Martínez

Abstract—Modular Arrays (MAs) are a promising architecture to enable multi-user communications in next-generation multiple-input multiple-output (MIMO) systems based on extra-large (XL) or gigantic MIMO (gMIMO) deployments, trading off an improved spatial resolution with characteristic interference patterns associated to grating lobes. In this work, we analyze whether MAs can outperform conventional collocated deployments, in terms of achievable sum-rate and served users in a multi-user downlink set-up. First, we provide a rigorous analytical characterization of the inter-user interference for modular gMIMO systems operating in the near field. Then, we leverage these results to optimize the user selection and precoding mechanisms, designing two algorithms that largely outperform existing alternatives in the literature, with different algorithmic complexities. Results show that the proposed algorithms yield over 70% improvements in achievable sum-spectral efficiencies compared to the state of the art. We also illustrate how MAs allow to serve a larger number of users thanks to their improved spatial resolution, compared to the collocated counterpart.

Index Terms—Modular arrays, near-field communications, user selection, massive MIMO, gigantic MIMO.

I. INTRODUCTION

MASSIVE Multiple-Input Multiple-Output (MIMO) technology is one of the key pillars for the success of fifth-generation (5G) wireless networks, and continuous efforts are made to improve its operation in the subsequent releases by 3rd Generation Partnership Project (3GPP) towards 5G-advanced [1]. As the different pathways to conceive the core technologies within the future sixth-generation (6G) standard are being discussed, the integration of an even larger number of antennas is facilitated when the operational frequency grows. Now, while academic research boldly advocates for moving beyond millimeter wave (mmWave) into subTHz bands [2], [3] to enable the Ultra Massive MIMO (UM-MIMO) concept, this could exacerbate the practical limitations of 5G commercial deployments in the Frequency Range (FR) of mmWave frequencies (FR2) [4]. Conversely, industry plays it safe and stands up for modest increases in the operational frequencies; in this sense, there seems to be a consensus that the so-called

upper midband (FR3) covering the 7-24 GHz range will play a central role in early 6G [5], [6], as confirmed by regulatory bodies such as the Federal Communications Commission (FCC) and International Telecommunications Union (ITU) [7], [8].

The evolution of antenna array technologies in the upper-midband allows to integrate thousands of antennas in a reasonable area at the Base Station (BS) side. This, combined with the use of distributed array deployments different than conventional collocated architectures [9]–[11], opens the door to extend the near-field (NF) features that enable beamfocusing to the entire operational range of the BS in 6G [6]. In this sense, the evolution of conventional collocated arrays to sparse or distributed deployments is shown to be beneficial for use cases like enhanced mobile broadband, localization and sensing. Recently, Modular Arrays (MAs) have been proposed [9], [10] in the context of extra-large (XL)-MIMO or gigantic MIMO (gMIMO) evolutions. This newly proposed architecture deploys multiple modules or sub-arrays with a moderate number of elements, classically spaced $\lambda/2$, with λ being the operational signal wavelength. Now, individual modules are separated much more than λ , thus increasing the overall array aperture. MA deployments are justified by the irregular shape of mounting structures like facades with windows, but also offer an alternative to implement coordinated transmission between sub-arrays with minimal synchronization requisites and a reduced backhaul overhead. Noteworthy, MAs allow the operation in the NF for a larger distance, even when individual sub-arrays may operate in the far-field (FF) zone. This offers an improved spatial resolution, at the expense of the appearance of grating lobes due to the large inter-module separation [12], which cause characteristic interference patterns that affect multi-user operation.

To avoid achievable sum-rate performance plummeting as the BS intends to serve a larger number of users, user selection¹ plays a pivotal role in the operation of multi-user communication systems. Selecting the set of users that will be allocated for transmission in the same time and frequency resource, and designing the corresponding precoding vectors and power allocation policies, is known to be a highly complex combinatorial and non-convex optimization problem, even when linear precoders are used [13]. The special features of NF propagation allow to better exploit the available spatial degrees-of-freedom (DoF) [14] which, in turn, allows for improved performance when taken into consideration in the

Manuscript received December xx, 2024; revised XXX. The review of this paper was coordinated by XXXX. This work is supported by grant PID2023-149975OB-I00 (COSTUME) funded by MICIU/AEI/10.13039/501100011033, and by ERDF/EU. The authors thank the Defense University Center at the Spanish Naval Academy for their support.

J.P. González-Coma is with the Defense University Center at the Spanish Naval Academy, 36920 Marín, Spain. Contact email: jose.gcoma@tud.uvigo.es.

S. Fernández and F.J. López-Martínez are with the Dept. Signal Theory, Networking and Communications, Research Centre for Information and Communication Technologies (CITIC-UGR), University of Granada, 18071, Granada, Spain.

¹Also referred to as user scheduling, user grouping, or user dropping in the literature.

user selection process [15]–[17]. For the specific case of MAs, this problem remains largely unexplored, and was only addressed in [12], where a greedy approach was explored to relax the computational burden. While showing some sum-rate improvements over the random user grouping case, it fails to provide a convincing performance when compared to state-of-the-art alternatives.

In this paper, we address the problem of user selection in the context of gMIMO systems equipped with MAs. First, we perform an analytical characterization of the multi-user interference patterns with MA deployments. This allows to obtain important insights related to the behavior of interference, which are later leveraged to design algorithms for joint user selection and precoding in this context. The performance and complexity of the proposed algorithms are evaluated in practical scenarios of gMIMO deployments in the upper mid-band, showing remarkable performance improvements over the greedy approach in [12].

The remainder of this paper is structured as follows: In Section II, the system model for a multi-user gMIMO system under spherical wavefront (SW) propagation is introduced. Then, the analytical characterization of the interference patterns is carried out in Section III. The algorithms for user selection and precoding design are presented in Section IV, and their performance and complexity are assessed in Section V. Finally, conclusions are outlined in Section VI.

Notation: a is a scalar, \mathbf{a} is a vector, and \mathbf{A} is a matrix. Transpose and conjugate transpose of \mathbf{A} are denoted by \mathbf{A}^T and \mathbf{A}^H , respectively. Calligraphic letters, e.g., \mathcal{A} denote sets and sequences. $|\mathcal{A}|$ represents the set cardinality and $\mathcal{A} \setminus \{b\}$ stands for the exclusion of b from \mathcal{A} , \odot and \otimes represent the Hadamard and the Kronecker product, respectively. Finally, the expectation operator is $E[\cdot]$ and $\|\cdot\|$ denotes the Euclidean norm.

II. SYSTEM MODEL

Let us consider a modular gMIMO setup deployed at the BS, where N modules composed by M antenna elements each form the array, hence consisting of a total of $N \times M$ elements as illustrated in Fig. 1. Without loss of generality, a modular Uniform Linear Array (ULA) is assumed to be placed along the y -axis, symmetric around the origin. For the sake of notation simplicity, we consider that the module index n and the antenna index m for each module belong to the integer sets $\mathcal{N} = \{0, \pm 1, \dots, \pm(N-1)/2\}$ and $\mathcal{M} = \{0, \pm 1, \dots, \pm(M-1)/2\}$. Consequently, the position of the m -th element within module n is $[0, (nS + m)d]^T$, $\forall n \in \mathcal{N}$, and $\forall m \in \mathcal{M}$. In the last expression, it is assumed a typical inter-element spacing for antennas within each module of half of the signal wavelength λ denoted by d , and S is the modular separation parameter, that may depend on the discontinuous surface of the practical installation structure, with $S \geq M$.

The position of the k -th user is then determined by the distance to the m -th element in module n and its angle with respect to the positive x -axis $\theta \in [-\pi/2, \pi/2]$, such that

$$r_{n,m} = \sqrt{r^2 - 2r(nS + m)d \sin \theta + (nS + m)d^2}, \quad (1)$$

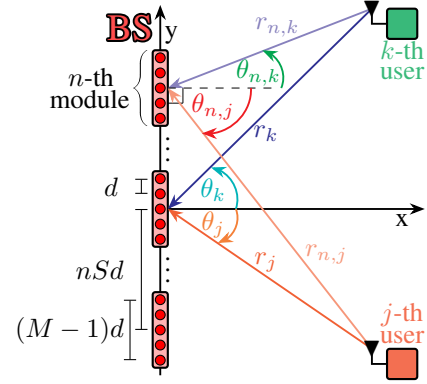


Fig. 1. A modular gMIMO system with N modules and M antennas in each module communicating with single-antenna users.

where r denotes its distance from the center of the antenna array.

Based on this formulation and assuming that the Line-of-Sight (LoS) component dominates the channel vector response [18], it is possible to write the channel model to accurately characterize the signal amplitude and phase variations over all elements of the $N \times M$ array for every k -th user as

$$\mathbf{h}(r, \theta) = \frac{\sqrt{\beta_0}}{r} \mathbf{a}(r, \theta), \quad (2)$$

where β_0 denotes the reference channel power gain at the distance of 1 meter (m), and the Array Response Vector (ARV) $\mathbf{a}_k \in \mathbb{C}^{N \times M}$ can be written as

$$\mathbf{a}(r, \theta) = \frac{r}{r_{n,m}} e^{-j \frac{2\pi}{\lambda} r_{n,m}}. \quad (3)$$

We also consider that the amplitude variations over all array elements can be neglected if $r \geq 1.2\Delta_{NM}$ [19], where $\Delta_{NM} = [(N-1)S + (M-1)]d$ is the total physical size of the modular gMIMO antenna array. Then, the position of the k -th user in (1) can be simplified to $\mathbf{a}(r, \theta) \approx e^{-j \frac{2\pi}{\lambda} r_{n,m}}$. Based on this observation and remembering that the boundary between FF and NF regions of antenna arrays can be pointed out based on the classical Rayleigh distance, i.e., $r_{\text{Ray}} = 2\Delta_{NM}^2/\lambda$, it is possible to express the ARV $\mathbf{a}(r, \theta)$ as a function of r based on the planar wavefront (PW) and the SW models for modular gMIMO antenna arrays.

A. Array response vector for modular arrays

In this work, we are interested in arrays in which the module sizes are small compared to the dimensions of the entire array, i.e., $2\Delta_M^2 \leq \lambda r < 2\Delta_{NM}^2$, where $\Delta_M = (M-1)d$ is the physical size of each module. In such a case, for a practical range of usage, the users are located within the NF region of the whole array, but within the FF region of each array module. In other words, there is no significant distance difference between users and adjacent antennas within a particular module. In contrast, the distance and Angle of Arrival (AoA) vary across different modules. In this way, the distance from the n -th module to a user located at a distance r and at an angle θ reads as

$$r_n = \sqrt{r^2 - 2rnSd \sin \theta + (nSd)^2} \quad \forall n \in \mathcal{N}, \quad (4)$$

Moreover, since θ_n represents the angle of the user to the center of each n -th module, it is defined

$$\sin \theta_n = \frac{r \sin \theta - nSd}{r_n} \quad \forall n \in \mathcal{N}. \quad (5)$$

Based on this geometrical model, the ARV can be compactly expressed as

$$\mathbf{a}(r, \theta) = (\mathbf{q}(r, \theta) \otimes \mathbf{1}_M) \odot \mathbf{u}(r, \theta), \quad (6)$$

where $\mathbf{q}(r, \theta) \in \mathbb{C}^{N \times 1}$ comprises the near-field delays as

$$\mathbf{q}(r, \theta) = \left[e^{-j \frac{2\pi}{\lambda} r_1}, \dots, e^{-j \frac{2\pi}{\lambda} r_N} \right]^T,$$

$\mathbf{1}_M$ is a column vector containing M ones, and $\mathbf{u}(r, \theta) = [\mathbf{b}^T(\theta_1), \dots, \mathbf{b}^T(\theta_N)]^T \in \mathbb{C}^{NM \times 1}$ with $\mathbf{b}(\theta_n) = [e^{j \frac{2\pi}{\lambda} m d \sin(\theta_n)}]_{m \in \mathcal{M}} \in \mathbb{C}^M$ for the n -th module represent the far-field effects within each of the modules. In the scenarios where the users are located on the FF region of the whole array, i.e. $r \geq r_{\text{Ray}}$, the first-order Taylor expansion can be used to approximate the distance expression in (4) as a linear function of the antenna index, so that $r_n \approx r - nSd \sin(\theta)$ and we get

$$\mathbf{q}(r, \theta) = e^{-j \frac{2\pi}{\lambda} r} \left[e^{-j \frac{2\pi}{\lambda} Sd \sin(\theta) \frac{N-1}{2}}, \dots, e^{j \frac{2\pi}{\lambda} Sd \sin(\theta) \frac{N-1}{2}} \right]^T. \quad (7)$$

Moreover, in this case, the angle is common for all the modules, i.e. $\theta_n \approx \theta$, such that $\mathbf{u}(r, \theta) = \mathbf{1}_N \otimes \mathbf{b}(\theta)$, and the array response vector simplifies to $\mathbf{a}(r, \theta) = \mathbf{q}(r, \theta) \otimes \mathbf{b}(\theta)$.

B. Problem formulation

In this work, we focus on a modular gMIMO setting. We consider that the BS communicates with the user $k \in \mathcal{K}$ by sending zero-mean data symbols $s_k \in \mathcal{N}_{\mathbb{C}}(0, 1)$. To enable the system's multi-user capabilities, the symbols are linearly processed with the unit-norm precoding vectors $\mathbf{p}_k \in \mathbb{C}^{NM \times 1}$. Thus, the transmitted signal is $\mathbf{x} = \sum_{k \in \mathcal{K}} \sqrt{p_k} \mathbf{p}_k s_k$, where p_k is the power allocated to the user, and we consider the total transmit power constraint $\sum_{k \in \mathcal{K}} p_k \leq P_{\text{TX}}$. The transmitted signal then inputs the wireless channel represented by the channel vector $\mathbf{h}(r_k, \theta_k)$ from (2) leading to the received signal of the k -th user

$$\begin{aligned} y_k &= \mathbf{h}^H(r_k, \theta_k) \mathbf{x} + z_k = \mathbf{h}^H(r_k, \theta_k) \sum_{k \in \mathcal{K}} \sqrt{p_k} \mathbf{p}_k s_k + z_k \\ &= \mathbf{h}^H(r_k, \theta_k) \sqrt{p_k} \mathbf{p}_k s_k + \mathbf{h}^H(r_k, \theta_k) \sum_{i \neq k} \sqrt{p_i} \mathbf{p}_i s_i + z_k \end{aligned} \quad (8)$$

where $z_k \in \mathcal{N}_{\mathbb{C}}(0, \sigma^2)$ is the noise. Note that the first term in (8) is the desired signal whereas the second one collects the inter-user interference (IUI). When the number of users grows large compared to NM , the achievable spectral efficiency (SE) is limited by the IUI, as can be noticed from

$$R_k = \log_2 \left(1 + \frac{p_k |\mathbf{h}^H(r_k, \theta_k) \mathbf{p}_k|^2}{\sum_{i \in \mathcal{S}, i \neq k} p_i |\mathbf{h}^H(r_k, \theta_k) \mathbf{p}_i|^2 + \sigma^2} \right), \quad (9)$$

where $\mathcal{S} \subseteq \mathcal{K}$ is the set of served users, i.e., those with $p_i > 0$. Two critical questions should then be addressed to solve this problem. First, it is of key importance to accurately

characterize the IUI according to the spatial positions of the users and then, according to such information, determine the set of users that are promising candidates to be served by the BS in each particular time-frequency resource block. The optimization problem is then formulated to maximize the achievable sum-SE as

$$\max_{\{\mathbf{p}_k\}_{k \in \mathcal{S}}} \sum_{k \in \mathcal{S}} R_k \quad \text{s.t.} \quad \sum_{k \in \mathcal{S}} p_k \leq P_{\text{TX}}. \quad (10)$$

In the next section, we analyze the dependence of IUI on the user positions to provide a first approach to solving the combinatorial problem in (10).

III. INTERFERENCE CHARACTERIZATION IN MAS

In this section, we study the consequences of employing a modular array architecture in terms of inter-user interference. For this purpose, we evaluate the interference caused by a user k located at a distance r_k and angle θ_k , to a different user j in the position given by r_j and θ_j from the general framework granted by the ARV in (6), as depicted in Fig. 1. Such IUI is determined by the similarity of ARVs, which is analyzed in the sequel. In particular, we are interested in the evaluation of the product $I(j, k) = \frac{1}{MN} |\mathbf{a}^H(r_j, \theta_j) \mathbf{a}(r_k, \theta_k)|$ as²

$$\begin{aligned} I(j, k) &= \frac{1}{MN} |((\mathbf{q}^H(r_j, \theta_j) \otimes \mathbf{1}_M^T) \odot \mathbf{u}^H(r_j, \theta_j)) \\ &\quad \times ((\mathbf{q}(r_k, \theta_k) \otimes \mathbf{1}_M) \odot \mathbf{u}(r_k, \theta_k))| \\ &= \frac{1}{MN} |\text{Tr} \{ (\mathbf{q}^H(r_j, \theta_j) \otimes \mathbf{1}_M^T) \text{diag}(\mathbf{u}^H(r_j, \theta_j)) \\ &\quad \times \text{diag}(\mathbf{u}(r_k, \theta_k)) (\mathbf{q}(r_k, \theta_k) \otimes \mathbf{1}_M) \}| \\ &\leq \frac{1}{MN} |\text{Tr} \{ (\mathbf{q}^H(r_j, \theta_j) \otimes \mathbf{1}_M^T) (\mathbf{q}(r_k, \theta_k) \otimes \mathbf{1}_M) \}| \\ &\quad \times |\text{Tr} \{ \text{diag}(\mathbf{u}^H(r_j, \theta_j)) \text{diag}(\mathbf{u}(r_k, \theta_k)) \}| \\ &= \frac{1}{N} |\mathbf{q}^H(r_j, \theta_j) \mathbf{q}(r_k, \theta_k)| \left| \sum_{n=1}^N \mathbf{b}^H(\theta_{j,n}) \mathbf{b}(\theta_{k,n}) \right|. \end{aligned} \quad (11)$$

The latter expression can be further bounded by taking the summation out of the absolute value, as follows

$$I(j, k) \leq \frac{1}{N} |\mathbf{q}^H(r_j, \theta_j) \mathbf{q}(r_k, \theta_k)| \sum_{n=1}^N |\mathbf{b}^H(\theta_{j,n}) \mathbf{b}(\theta_{k,n})|. \quad (12)$$

Observe that when the inner products present identical sign for all n , (12) is equal to the bound in (11). This situation also arises when the angles for the different modules are the same, i.e., $\theta_n = \theta$. In addition, a simplified version of $I(j, k)$ in (12) is useful when both users lie on the FF region, or under the assumption $\theta_n \approx \theta$. For such a case we have that

$$\begin{aligned} I(j, k) &= \frac{1}{MN} |\mathbf{q}^H(r_j, \theta_j) \mathbf{q}(r_k, \theta_k) \otimes \mathbf{b}^H(\theta_j) \mathbf{b}(\theta)| \\ &= \frac{1}{MN} |\mathbf{q}^H(r_j, \theta_j) \mathbf{q}(r_k, \theta_k) \mathbf{b}^H(\theta_j) \mathbf{b}(\theta_k)| \\ &= \frac{1}{MN} |\mathbf{q}^H(r_j, \theta_j) \mathbf{q}(r_k, \theta_k)| |\mathbf{b}^H(\theta_j) \mathbf{b}(\theta_k)|. \end{aligned} \quad (13)$$

²The product $I(j, k)$ coincides with the IUI caused by a Maximum Ratio Transmission (MRT) precoding scheme up to a scale factor, i.e., $\mathbf{p}_k = \mathbf{a}(r_k, \theta_k)$ and hence the denominator of (9) reads as $|\mathbf{h}^H(r_j, \theta_j) \mathbf{p}_k|^2 = \frac{\beta_0}{r_j^2} |\mathbf{a}^H(r_j, \theta_j) \mathbf{a}(r_k, \theta_k)|^2$.

In moving from (12) to (13) we split the interference into two parts: *i*) one corresponding to the module separation, and *ii*) a second factor corresponding to the modules themselves. Thus, both expressions present products which depend on vectors with unit-norm elements, but very different sizes. Indeed, the scenario of interest is such that where $N \gg M$, in such a way that it makes it possible to consider the individual modules achieving the conditions of far-field propagation. In contrast, the distance between the modules incorporates the effects of the near-field propagation environment. Accordingly, the interference mitigation capabilities within each module are limited compared to that of the modular array. This is because the vector space of dimension N allows much more flexibility to handle interference than the one of dimension M corresponding to the modules. Therefore, the following subsections allow us to draw relevant conclusions for the approximation in (12) and the exact reformulation of (13).

A. Inter-module interference

We now study the first factor in (12) and (13), $|\mathbf{q}^H(r_j, \theta_j)\mathbf{q}(r_k, \theta_k)|$ to evaluate the impact of user location on the IUI, i.e.,

$$\frac{1}{N}|\mathbf{q}^H(r_j, \theta_j)\mathbf{q}(r_k, \theta_k)| = \frac{1}{N} \left| \sum_{n \in \mathcal{N}} e^{j\frac{2\pi}{\lambda}(r_{k,n} - r_{j,n})} \right|, \quad (14)$$

where $r_{k,n}$ and $r_{j,n}$ represent the distance from the n -th module to user k and j , respectively. A closed-form expression for this equation is difficult to achieve due to the complicated definition of the module distances in (4). Nevertheless, different approximations can be employed to arrive at analytical forms for each possible scenario, as formally stated in the following proposition.

Proposition 1. *The effect of module separation on IUI can be approximated as*

$$\frac{1}{N}|\mathbf{q}^H(r_j, \theta_j)\mathbf{q}(r_k, \theta_k)| \approx \frac{1}{N\sqrt{2a}} |F(t^+) - F(t^-)|, \quad (15)$$

with parameters $a > 0$ and b dependent on user locations, $t^- = -\frac{a}{\sqrt{2}} + \frac{b}{\sqrt{2a}}$ and $t^+ = \frac{a}{\sqrt{2}} + \frac{b}{\sqrt{2a}}$, and $F(\cdot)$ being the Fresnel function $F(\tau) = \int_0^\tau [\cos(\frac{\pi}{2}t^2) + j \sin(\frac{\pi}{2}t^2)] dt$ [20].

Proof. See Appendix A. \square

Some features of the Fresnel function are helpful to identify convenient ranges of values for a and b . Specifically: *i*) $F(0) = 0$; *ii*) $F(x)$ is an odd function which quickly increases with $x > 0$; and *iii*) $F(x)$ is upper bounded by 0.95 and converges to $\frac{1}{\sqrt{2}}$ as x becomes large. In the ensuing subsections, we explore the values of a and b for several practical situations to achieve insight regarding the influence of user locations over inter-user interference. This information will lead to later define geometry-based strategies for selecting users in a scheduling procedure.

1) *Interference in the NF region:* When both users lie on the NF region, the second-order Taylor approach of the module distances leads to tractable expressions for the interference [21], [22]. In particular, the parameters a and b of the resulting

quadratic form are closely related to the geometrical features of the scenario, as follows

$$a = \frac{1}{\lambda} N^2 S^2 d^2 \left(\frac{\cos^2(\theta_k)}{r_k} - \frac{\cos^2(\theta_j)}{r_j} \right), \quad (16)$$

$$b = -\frac{2}{\lambda} N S d (\sin(\theta_k) - \sin(\theta_j)). \quad (17)$$

When performing scheduling tasks, it is usually desirable to find sets of users with negligible or even zero IUI. This can be achieved when (15) is small. A reduced value for the numerator of (15) can be achieved when the parameters a and b satisfy, simultaneously, the next conditions

$$b \approx a\sqrt{a}, \quad b \approx -a\sqrt{a}, \quad (18)$$

so that $F(t^+) - F(t^-) \approx 0$. This situation is only met with equality when $a = b = 0$. However, this situation would cause an indetermination in (15) as a also appears in the denominator. Also, recall that we assume $a > 0$ in Appendix A, so we cannot achieve (18) with an arbitrarily small precision. From a geometrical point of view, $a = b = 0$ in (16) and (17) would imply the trivial case on which the positions of the two users are identical, that lacks practical interest. Alternatively, as the numerator of (15) is bounded, the interference can be reduced by increasing the denominator

$$\sqrt{2a} = \sqrt{\frac{2}{\lambda}} N S d \left(\frac{\cos^2(\theta_k)}{r_k} - \frac{\cos^2(\theta_j)}{r_j} \right)^{1/2}. \quad (19)$$

Note that this happens when the user locations differ. For instance, selecting users such as $r_k \gg r_j$ might reduce the interference, but the channel for the furthest user will be poor due to path loss. Hence, it is interesting to select users located at distances in the same order of magnitude, $r_k \approx r_j$, but θ_k and θ_j such that the difference of cosines is as large as possible. Interestingly, the module separation S increases the number of grating lobes but linearly increases the denominator of the interference function of (15), that is (19), then resulting in a trade-off. Also, a larger number of modules, i.e. increasing N , contributes to reducing the interference. From a geometrical perspective, we arrive at a similar conclusion, since for users located at similar distances to the BS, $r_k \approx r_j$, only the negative term in (4) for $r_{k,n}$ and $r_{j,n}$ significantly changes from the module distances of the two interferent users.

To better illustrate our observation and provide further insight, we consider the scenario where a user is located at a distance r_k and $\theta_k = 0$ (i.e., located over the x -axis), with r_k and r_j being comparable. Thus, the denominator of the interference function of (15), $\sqrt{2a}$ in (19), can be approximated by

$$\sqrt{2a} \approx \sqrt{\frac{2}{\lambda r_j}} N S d |\sin(\theta_j)|. \quad (20)$$

As we desire to get large values for (20) in order to reduce the interference, and under the aforementioned assumptions, we seek users with angular coordinate θ_j away from zero but, at the same time, a value r_j as small as possible.

2) *Interference in NF and FF regions:* When users close to the BS are not eligible to be scheduled for transmission, it is interesting to check the interference caused to those users in the region where the FF condition holds. In this case, one of the ARVs obeys (7), and the difference of distances can be written as $r_{k,n} - r_{j,n} = r_{k,n} + nSd \sin(\theta_j)$. Using the second-order Taylor approach for the NF user as in Appendix A, we characterize the interference with the approximation in (15) by updating the values of a and b accordingly, that is,

$$a = \frac{1}{\lambda} N^2 S^2 d^2 \left(\frac{\cos^2(\theta_k)}{r_k} \right), \quad (21)$$

whereas b is that in (17). If we consider the user in the NF region fixed, the condition in (18) can be recasted to

$$\theta_j \approx \arcsin \left(\sin(\theta_k) \pm \frac{N^2 S^2 d^2}{2r \sqrt{r_k \lambda}} \cos^3(\theta_k) \right).$$

Since the assumption of a given user in the NF region keeps the denominator in (15) fixed, feasible values of θ_j critically depend on θ_k , as very small values on $\cos^3(\theta_k)$ are interesting to achieve a smaller amount of interference on users located in the FF region. Due to the dependence on r_k , this effect is stronger when the user in the NF region is closer to the BS.

If we consider the opposite scenario, that is, a given user in the FF and a low interference candidate in the NF counterpart, strong candidates to be scheduled are those users with a reduced value of r_k and a large value for $\cos^2(\theta_k)$. In other words, users close to the broadside of the BS.

3) *Interference in the FF region:* When both users are located at a significant distance to the BS, the vectors in (7) accurately represent inter-module delays, and the product can be written using the well-known expression

$$\frac{1}{N} |\mathbf{q}^H(r_j, \theta_j) \mathbf{q}(r_k, \theta_k)| = \left| \frac{\sin\left(\frac{\pi}{2}(NS(\sin(\theta_k)) - \sin(\theta_j))\right)}{N \sin\left(\frac{\pi}{2}S(\sin(\theta_k) - \sin(\theta_j))\right)} \right|. \quad (22)$$

In contrast with the NF scenario in Sec. III-A1, this interference only depends on the user angles θ_k and θ_j . While in the NF scenario the module separation S increases the denominator in the interference expression and hence increases (19), in the FF case S denotes the number of grating lobes in the radiation pattern of the antenna array, thus reducing the angular directions experiencing low interference. Accordingly, we can expect stronger interference in the FF as the ARVs are independent of the distance, and there is no counterpart for balancing the effects of the grating lobes.

B. Intra-module interference

Thus far, we have studied the first factor within the interference bound in (12), associated to inter-module interference.

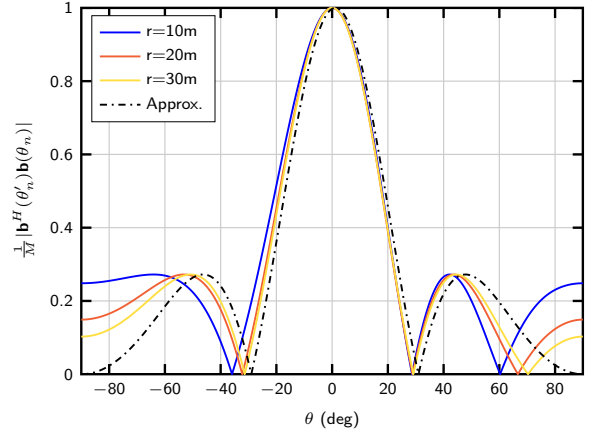


Fig. 2. Worst case scenario for the common angle approximation. Parameter values are $N = 32$, $M = 4$, $S = 13$, $f_c = 15\text{GHz}$. The proposed bound is 22.3734 m for the considered setup.

We now study the second factor caused by the intra-module interaction. The general expression for this factor reads as

$$\begin{aligned} & \frac{1}{M} |\mathbf{b}^H(\theta_{j,n}) \mathbf{b}(\theta_{k,n})| \\ &= \frac{1}{M} \left| \sum_{m \in \mathcal{M}} e^{j \frac{2\pi}{\lambda} m d (\sin(\theta_{k,n}) - \sin(\theta_{j,n}))} \right| \\ &= \frac{1}{M} \left| \frac{\sin\left(M \frac{\pi}{\lambda} d (\sin(\theta_{k,n}) - \sin(\theta_{j,n}))\right)}{\sin\left(\frac{\pi}{\lambda} d (\sin(\theta_{k,n}) - \sin(\theta_{j,n}))\right)} \right|. \quad (23) \end{aligned}$$

It is interesting to determine the geometrical region where the bound of (12) becomes tight. A similar region was defined in [23], but led to a very pessimistic bound that can be further enhanced. In particular, we characterize the region for which it becomes reasonable to consider that $\theta_{k,n} \approx \theta_k$, where θ_k is the angular position of the user and $\theta_{k,n}$ the angle of the user to the center of each n -th module. To determine such a region, we use a criterion similar to that employed to obtain the half-power beamwidth, now with a 5% power reduction for increased accuracy. This is formally stated in the following Proposition.

Proposition 2. (Common angle approximation)

The distance r for which $\frac{1}{M} |\mathbf{b}^H(\theta_k) \mathbf{b}(\theta_{k,n})| \approx 0.95$ is given by

$$r \geq \frac{(N-1)Sd}{2\epsilon}, \quad (24)$$

with $\epsilon = -\frac{2}{M} 0.18$.

Proof. See Appendix B. \square

Note the dependency in Proposition 2 on the number of elements per module M , which linearly increases the minimum distance, as the angular resolution also scales linearly with this parameter. The accuracy of this approximation is illustrated numerically in Fig. 2, where the conservative approximation for the module $n = \frac{(N-1)}{2}$ is shown.

According to the previous discussion, the intra-module factor has to be characterized with respect to the bound (24). In particular, when the distances for both users satisfy (24) we

have that equation (11) (and (12) as a consequence) reduces to (13), where the two factors contributing to the interference are decoupled and can be analyzed independently.

IV. USER SELECTION AND PRECODING DESIGN

The comprehensive characterization of interference patterns in gMIMO deployments based on MAs provides a solid foundation for the design of joint user selection and precoding schemes. Based on these features, two user selection algorithms are designed and described next, together with an algorithmic description for each of them.

A. Algorithm 1: RSS.

The first algorithm, referred to as Rectangular-Search Scheduler (RSS), leverages the insights presented in Sec. III, as user location in the area covered by the BS is a fundamental factor in the eligibility for such a user. Accordingly, the RSS method starts by selecting a rectangular-shaped area to discriminate the potential users, where l sets the limit on both the horizontal and vertical axes, making an overall search area of $2l^2$. Thanks to this separation, it is possible to avoid an extensive search containing all users. As we will later see, such a restriction notably reduces the complexity with a minor performance degradation. Once the search area is determined, the user with a minimum horizontal coordinate is selected. This is in coherence with the analysis of the interference in the NF region in Sec. III, that promotes users with lower horizontal coordinates with the aim of reducing IUI. To check whether a given user stands out as a low IUI candidate, we use the following metric

$$\gamma_{\text{eq},k} = \|\mathbf{h}_k\|_2^2 / \left(\mathbf{h}_k^H (\mathbf{I} - \sum_{i=1}^n \mathbf{f}^{(i)} \mathbf{f}^{H,(i)}) \mathbf{h}_k \right), \quad (25)$$

where $\mathbf{f}^{(i)}$ denotes a tentative precoding vector employed during the determination of the set of active users \mathcal{S} . In particular, at the iteration n of the algorithm, the ZF precoder is computed for the selected user k , as follows

$$\mathbf{f}^{(n)} = \alpha_k (\mathbf{I} - \mathbf{H}_{\bar{k}} (\mathbf{H}_{\bar{k}}^H \mathbf{H}_{\bar{k}})^{-1} \mathbf{H}_{\bar{k}}^H) \mathbf{h}_k, \quad (26)$$

where $\mathbf{H}_{\bar{k}} = \{\mathbf{h}_i\}_{i \in \mathcal{S}, i \neq k}$ and α_k guarantees that $\mathbf{f}^{(n)}$ is unit-norm.

The ratio $\gamma_{\text{eq},k}$ provides information regarding the amount of IUI suffered by user k , with a denominator that penalizes users whose channel vectors exhibit high correlation with those already marked as active. In particular, the user is included in the set of active users \mathcal{S} if $\gamma_{\text{eq},k}$ is above a given threshold μ . This value can be adapted depending on the scenario, to serve users by adjusting the tolerable amount of interference. The algorithm then continues selecting users from the rectangular area earlier determined, until there are no more eligible users. Next, the rectangular area is increased and the selection procedure starts again. The method stops when the stopping criterion is met. When the procedure for joint user selection and precoding ends, the set \mathcal{S} is fully determined and the actual precoders in (8) are found as

$$\mathbf{p}_k = \alpha_k (\mathbf{I} - \mathbf{H}_{\bar{k}} (\mathbf{H}_{\bar{k}}^H \mathbf{H}_{\bar{k}})^{-1} \mathbf{H}_{\bar{k}}^H) \mathbf{h}_k. \quad (27)$$

As a final step, the power allocation coefficients p_k are computed using the waterfilling procedure.

Algorithm 1 Rectangular-Search Scheduler (RSS)

```

1:  $n \leftarrow 0$ ,  $\mathcal{S}^{(0)} \leftarrow \emptyset$ ,  $\mathcal{K}^{(0)} \leftarrow \{1, \dots, K\}$ ,  $l \leftarrow$  initialization
2: repeat
3:    $\mathcal{R} \leftarrow \{i \in \mathcal{K}^{(n)} | x_i < l, |y_i| < l\}$ 
4:   repeat
5:      $k \leftarrow \min_{i \in \mathcal{R}} x_i$ 
6:      $\mathcal{R} \leftarrow \mathcal{R} \setminus \{k\}$ 
7:      $\gamma_{\text{eq},k} \leftarrow \|\mathbf{h}_k\|_2^2 / (\mathbf{h}_k^H (\mathbf{I} - \sum_{i=1}^n \mathbf{f}^{(i)} \mathbf{f}^{H,(i)}) \mathbf{h}_k)$ 
8:     if  $\gamma_{\text{eq},k} \geq \mu$  then
9:        $n \leftarrow n + 1$ 
10:       $\mathcal{S}^{(n)} \leftarrow \mathcal{S}^{(n-1)} \cup \{k\}$ 
11:       $\mathbf{f}^{(n)} \leftarrow$  Compute ZF precoder for user  $k$ 
12:       $\mathcal{K}^{(n)} \leftarrow \mathcal{K}^{(n-1)} \setminus \{k\}$ 
13:    end if
14:  until  $\mathcal{R} = \emptyset$ 
15:   $l \leftarrow l + 1$ 
16: until  $\mathcal{K}^{(n)} = \emptyset$  or stopping criterion

```

Algorithm 2 Front Line Scheduler (FLS)

```

1:  $n \leftarrow 0$ ,  $\mathcal{S}^{(0)} \leftarrow \emptyset$ ,  $\mathcal{K}^{(0)} \leftarrow \{1, \dots, K\}$ 
2: repeat
3:    $k \leftarrow \min_{i \in \mathcal{K}^{(n)}} x_i$ 
4:    $\gamma_{\text{eq},k} \leftarrow \|\mathbf{h}_k\|_2^2 / (\mathbf{h}_k^H (\mathbf{I} - \sum_{i=1}^n \mathbf{f}^{(i)} \mathbf{f}^{H,(i)}) \mathbf{h}_k)$ 
5:   if  $\gamma_{\text{eq},k} \geq \mu$  then
6:      $n \leftarrow n + 1$ 
7:      $\mathcal{S}^{(n)} \leftarrow \mathcal{S}^{(n-1)} \cup \{k\}$ 
8:      $\mathbf{f}^{(n)} \leftarrow$  Compute ZF precoder for user  $k$ 
9:      $\mathcal{K}^{(n)} \leftarrow \mathcal{K}^{(n-1)} \setminus \{k\}$ 
10:  end if
11: until  $\mathcal{K}^{(n)} = \emptyset$  or stopping criterion

```

B. Algorithm 2: FLS.

The method proposed in Alg. 1 uses a rectangular-shaped area, which represents a trade-off between the IUI due to the modular array beam pattern and the user distance r_k . According to (2), this distance is inversely proportional to the achievable SINR of the user, and determines the attainable performance.

In order to reduce complexity, a simplified version of Alg. 1 referred to as Front Line Scheduling (FLS) is presented in Alg. 2, where only the amount of IUI is considered in the search of candidate users. Hence, this simplification avoids defining a rectangular area and directly evaluates users based on their position over the horizontal axis. This simpler version is more efficient, although its performance depends on the scenario under consideration. Specifically, for users located far away in the vertical axis, FLS will prioritize serving such users over other candidates with larger equivalent channel gains, which are closer to the BS.

C. A note on complexity.

The computational cost of (26) is high, especially due to the computation of the matrix inversion and the matrix products within the inverse operation, with complexity costs in the order of $\mathcal{O}(|\mathcal{S}|^3)$ and $\mathcal{O}(|\mathcal{S}|^2 MN)$, respectively, where $|\mathcal{S}|$ is the number of served users [24]. Hence, these calculations become the performance bottleneck when a large number of users is checked in the selection procedure. To reduce such complexity, it is possible to approximate the computation of the inverse as

in [24], [25], which entails a performance loss inherent to the approximation. In this work, we propose an alternative *exact* procedure that takes advantage of the iterative structure of the Gram matrix $\mathbf{H}_k^H \mathbf{H}_k$. This novel procedure, which is detailed in Appendix C, allows to obtain the exact matrix inversion with a computational cost of about $\mathcal{O}(|\mathcal{S}|MN)$, which is linear on both the number of users and antennas.

V. NUMERICAL RESULTS

In this section, we conduct numerical experiments to assess the performance benefits of the proposed methods. We consider a carrier frequency $f_c = 15$ GHz in the FR3 band, due to its promising balance between bandwidth availability and coverage [6]. Unless otherwise stated, we consider a scenario where the BS is equipped with a modular array with $N = 32$ modules of $M = 4$ antennas each with a separation parameter $S = 13$, attempting to serve $K = 300$ users, and the reference channel power gain is $\beta_0 = 0$ dB.

According to the spatial features of the test environment defined in [26] for evaluating 5G radio technologies in an urban environment with high user density, we consider a first scenario where users are uniformly distributed inside an area for which $r_k \in [10, 60]$ m and $\theta_k \in [-60^\circ, 60^\circ]$, with SNR values ranging from 0 to 25 dB. For benchmarking purposes, we compare our results with some recent methods, namely: (i) Distance-Based Scheduling (DBS) in [15]; (ii) the greedy approach in [23], labeled as Greedy in the figures; and (iii) the classical successive user selection (SUS) scheme [13]. The collocated configuration with $S = M$ is used analyzed as a reference. It is worth mentioning that all these benchmark methods avoid the combinatorial nature of the problem in (10) in different ways: on the one hand, SUS in [13] explores all the available users to find the best-fitting candidate at each step. Conversely, the greedy method in [23] (specifically designed modular arrays) randomly selects a user and computes the achievable sum rate to ensure that a performance gain is obtained. This notably speeds up the search step, although performance is limited due to the random user selection scheme. Finally, the DBS method in [15] uses the distance from the user to the BS as a channel quality indicator to reduce the number of candidate users. However, this strategy neglects the specific patterns of modular arrays, and sectorized user locations.

Fig. 3 shows the average sum spectral efficiency for the different scheduling strategies. As one can notice, the proposed methods achieve results very close to that of the SUS benchmark of [13], which checks all the available users at each iteration. Hence, using the insights from the interference analysis performed in Sec. III allows that the definition of a spatial region of interest dramatically reduces the number of candidate users, with a minor performance degradation. As observed in (19), users with angular coordinate θ away from 0 suffer from less interference and they are therefore easier to accommodate in the scheduling procedure. At the same time, the channel gains are directly related to the distance to the BS r_k , and the rectangular area employed by the RSS proposal constitutes a compromise between these two

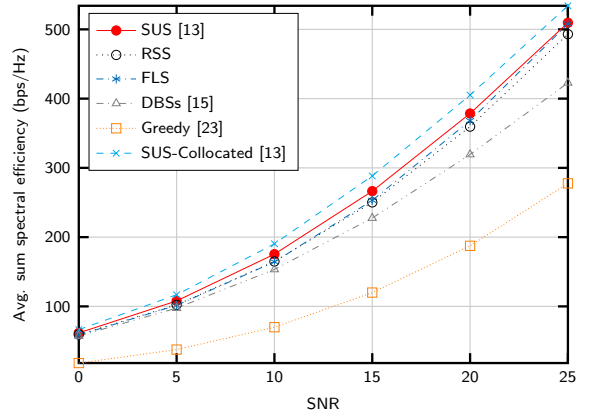


Fig. 3. Sum SE vs. SNR for the different schemes. $N = 32$, $M = 4$, $K = 300$, $S = 13$, $f_c = 15$ GHz, $r_k \in [10, 60]$ m and $\theta_k \in [-60^\circ, 60^\circ]$.

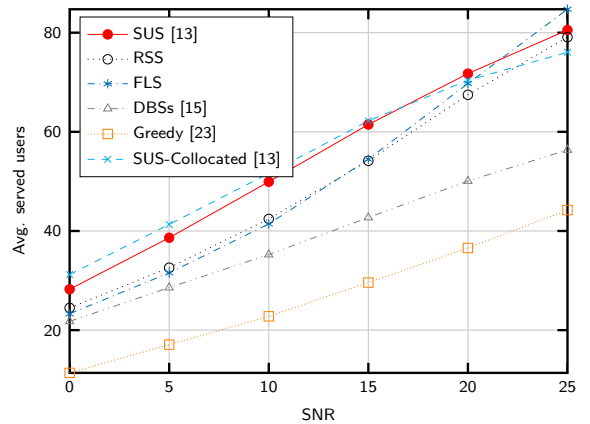


Fig. 4. Number of served users vs. SNR for the different schemes. $N = 32$, $M = 4$, $K = 300$, $S = 13$, $f_c = 15$ GHz, $r_k \in [10, 60]$ m and $\theta_k \in [-60^\circ, 60^\circ]$.

criteria. The simpler FLS scheme selects users disregarding the distance criterion, since the difference in the angular domain helps to alleviate the interference, thus enhancing the speed of the procedure. The DBS method [15] only relies on the distance r_k to prioritize users, thus reducing the computational cost but penalizing the overall performance results, while the random assignment of the algorithm in [23] leads to the worst performance result. Finally, we note that the achievable throughput with a collocated configuration provides the largest SE in this context due to milder IUI caused by the absence of grating lobes.

In Fig. 4, we analyze the number of served users for each of the competing schemes. It becomes evident that curves show a similar trend as in Fig. 3, since we can expect that a larger number of served users leads to better performance. However, it is interesting to see that the use of modular arrays allows to serve a larger number of users that under the collocated array counterpart in the large SNR regime. This is due to the improved spatial resolution provided by modular arrays, which allows to have a better control over the IUI. For lower SNRs, the energy spread due to the grating lobes results in poorer channel gains for the modular arrangement, and the number of users being served is smaller than for the collocated

TABLE I
EXECUTION TIME (MS)

Method/SNR(dB)	0	5	10	15	20	25
SUS	38.2	50.9	66.3	78.8	97.3	111.8
Greedy	2.11	4.02	6.39	9.08	12.61	20.08
RSS	5.81	8.81	12.82	14.53	20.46	28.21
DBS	4.93	7.07	9.17	11.45	14.53	15.40
FLS	5.28	7.68	11.91	14.33	20.22	30.11

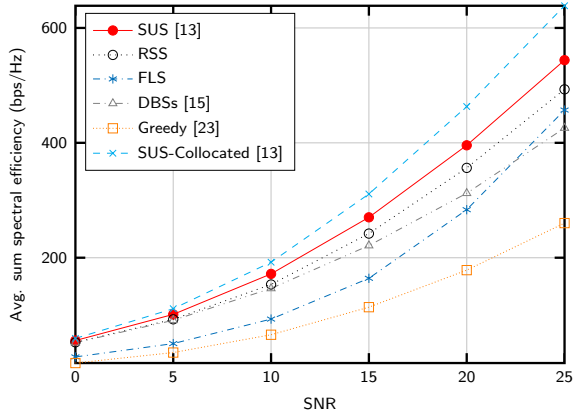


Fig. 5. Sum SE vs. SNR for the different schemes. $N = 32$, $M = 4$, $K = 300$, $S = 13$, $f_c = 15$ GHz, coordinates $x \in [10, 60]$ m, and $y \in [-60, 60]$ m.

counterpart.

To further illustrate the benefits of the proposed user selection schemes, the execution times for all competing methods are included in Table I. In all instances, the SUS method requires the largest computational effort. The RSS provides the best trade-off performance between complexity and performance, providing over a 75% reduction compared to the SUS scheme. In general terms, the FLS algorithm should allow for an even more reduced execution time; however, since this strategy allows to serve a larger number of users for high SNR, such a reduction may be overshadowed by the fact that complexity is proportional to the cardinality of $|\mathcal{S}|$. The reference greedy scheme developed in [23] allows for a reduced execution time, at the expense of a rather low performance. Finally, the DBS also offers a limited complexity, although its performance is below the RSS and FLS schemes.

In Fig. 5, we now analyze the achievable performance in a second scenario inspired in [27]. We consider that users are uniformly located within a rectangular area with cartesian coordinates $x \in [10, 60]$ m, and $y \in [-60, 60]$ m, while keeping the remaining setup parameters. Compared to the previous scenario under consideration, a larger area is covered by the BS, which severely affects the spatial positions for the candidate users. We can observe from Fig. 5 that the performance of FLS drops, since neglects distance to the BS to select candidate users. Remarkably, RSS still performs very close to the more complex SUS. It is also interesting to see that having a larger area close to the BS lessens the amount of interference. This favors the collocated configuration (which has a wider angular resolution) over the modular arrangement, exhibiting the former a superior performance.

In Fig. 6, the spatial distribution for the set of selected users is represented, for each of the scenarios under consideration. Specifically, users selected for transmission under the reference SUS scheme are represented with red crosses, while users within the service area are depicted using black triangles. This figure is useful to confirm the intuition behind the RSS scheme, since virtually all users selected by the SUS scheme lie within a rectangular-shaped area, represented with dashed lines. Hence, reducing the number of candidate users has a limited impact on performance, while notably reducing the search space and hence the overall complexity.

We now aim to explore the performance of the user selection schemes as users are farther away from the BS, to assess the performance of modular arrays when the benefits of beamfocusing are less evident. First, we study the evolution of the interference pattern for two users located at the same distance r to the BS. One of the users is located at $\theta = 0$ whereas the other one ranges from angular locations between -90° and 90° . In Fig. 7, we represent the evolution of the radiation pattern as a function of the angular location of the second user, with the case of PW propagation included as a reference. As r grows, the angular resolution is reduced and the behavior tends to coincide with that of the PW case, especially for low values of θ .

Based on these observations, we assess the achievable performance of the different scheduler competitors in Fig. 8. Simulation parameters are the same as in Fig. 3, but we modify the user distance range to $r_k \in [60, 150]$ m. Recall that the scheduling strategies RSS and FLS are designed for mitigating the IUI in the NF region, according to the observations in Sec. III. Hence, they cannot leverage the SW features as users are closer to the FF region, and their achievable performance is affected. However, the RSS technique still offers a reasonably good performance compared to all competitor schemes, while FLS and DBS improve the greedy scheme in [23]. Noteworthy, the modular and collocated configurations exhibit a similar behavior in this scenario, since the selection of users in regions affected by the grating lobes becomes less likely.

VI. CONCLUDING REMARKS

In this work, we characterized the IUI generated in a communication system composed of a modular gMIMO array, being able to quantify the impacts of inter-module and intra-module interferences inherent to this novel configuration. This result was then used to address the problem of user selection and precoding, designing feasible low-complexity strategies that leverage the spatial interference patterns when modular arrays are used. Performance was evaluated in a number of scenarios of interest in the FR3 band, showing that the proposed algorithms behave close to the reference SUS scheme, and largely outperform existing methods in the literature. Results confirm that the narrower spatial resolution of modular arrays allows to serve a larger number of users, and that the techniques to reduce the cardinality of the search space of potentially eligible users provide a significant decrease in the computational burden.

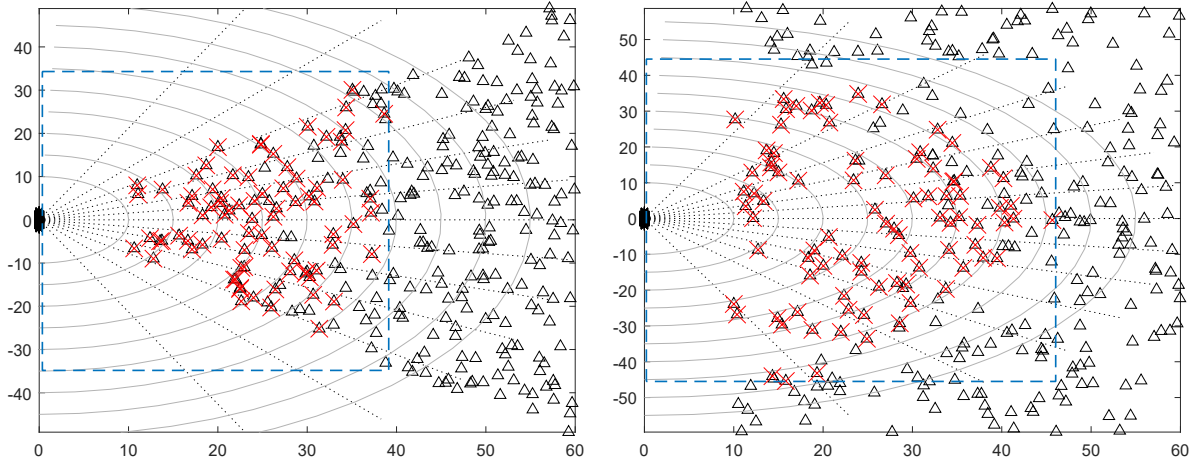


Fig. 6. User distributions for the considered setups. On the left figure we show the environment defined in [26] for evaluating 5G radio technologies in an urban environment with high user density. The right figure deploys the users in a rectangular area according to setups defined in [27].

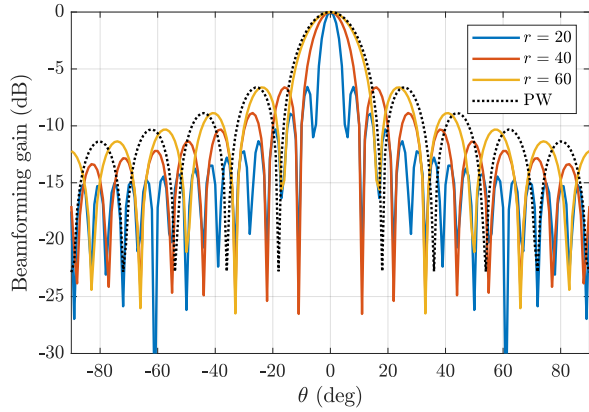


Fig. 7. Interference (BF gain) suffered by a user located at a distance r and angle θ when transmitting to a user located at the same distance and angle 0, for $N = 32$, $M = 4$, $S = 13$, $f_c = 15$ GHz.

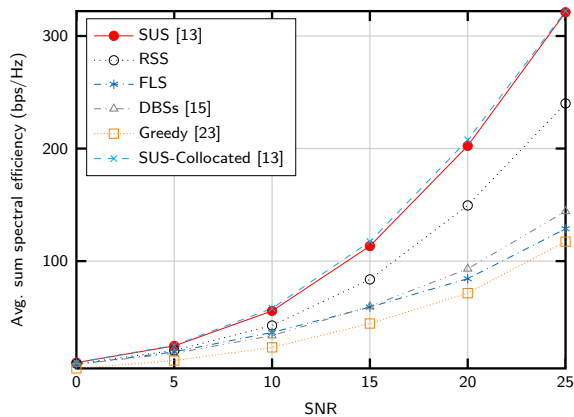


Fig. 8. Sum SE vs. SNR for the different schemes. $N = 32$, $M = 4$, $K = 300$, $S = 13$, $f_c = 15$ GHz, $r_k \in [60, 120]$ m and $\theta_k \in [-60^\circ, 60^\circ]$.

APPENDIX A FRESNEL INTEGRAL

First, we apply the second-order Taylor approach to $r_{k,n}$ and $r_{j,n}$ as a function of the module index n , leading to

$r_{k,n} - r_{j,n} \approx \frac{\lambda}{2}(\bar{a}n^2 + \bar{b}n)$. Then, the right-hand side of (14) is approximated as

$$\begin{aligned} \frac{1}{N} \left| \sum_{n \in \mathcal{N}} e^{j\frac{2\pi}{\lambda}(r_{k,n} - r_{j,n})} \right| &\approx \frac{1}{N} \left| \sum_{n \in \mathcal{N}} e^{j\pi(\bar{a}n^2 + \bar{b}n)} \right| \\ &\approx \frac{1}{N} \left| \int_{-\frac{1}{2}}^{\frac{1}{2}} e^{j\pi(ax^2 + bx)} dx \right|, \end{aligned} \quad (28)$$

Note that we can assume $\bar{a} > 0$ without loss of generality. Further, in the second line of (28) the summation is approximated by a continuous integral in $x \in [-\frac{1}{2}, \frac{1}{2}]$ such that $x = \frac{n}{N}$ [28], with $a = N^2\bar{a}$ and $b = N\bar{b}$. Note that this approximation holds tight for large values of N . At this point, it is useful to rewrite the exponent of the integral as follows

$$\left| \int_{-\frac{1}{2}}^{\frac{1}{2}} e^{j\pi(ax^2 + bx)} dx \right| = \left| \int_{-\frac{1}{2}}^{\frac{1}{2}} e^{j\pi a \left(x + \frac{b}{2a}\right)^2} dx \right|$$

which can be expressed, after a change of variables, as

$$\begin{aligned} \int_{-\frac{1}{2}}^{\frac{1}{2}} e^{j\pi a \left(x + \frac{b}{2a}\right)^2} dx \\ = \frac{1}{\sqrt{2a}} \int_{t^-}^{t^+} \left[\cos\left(\frac{\pi}{2}t^2\right) + j \sin\left(\frac{\pi}{2}t^2\right) \right] dt \end{aligned}$$

with the integration limits t^- and t^+ as defined in Prop. 1. Finally, using the definition of the Fresnel function $F(x)$ we get

$$\left| \int_{-\frac{1}{2}}^{\frac{1}{2}} e^{j\pi(ax^2 + bx)} dx \right| = \frac{1}{\sqrt{2a}} |F(t^+) - F(t^-)|,$$

which completes the proof.

APPENDIX B GEOMETRIC AREA FOR THE APPROXIMATION IN PROP. 2

We aim at finding the geometric area where the approximation of Prop. 2 is tight, i.e., $\frac{1}{M} |\mathbf{b}^H(\theta)\mathbf{b}(\theta_n)| \approx 0.95$. By

letting $\sin(\theta_n) = \sin(\theta) + \epsilon$, and using $d = \lambda/2$ for simplicity, the inner product of these vectors can be written as

$$\left| \frac{\sin\left(\frac{\pi}{2}M(\sin(\theta_n) - \sin(\theta))\right)}{M \sin\left(\frac{\pi}{2}(\sin(\theta_n) - \sin(\theta))\right)} \right| = \left| \frac{\sin\left(\frac{\pi}{2}M\epsilon\right)}{M \sin\left(\frac{\pi}{2}\epsilon\right)} \right| \approx \left| \frac{\sin\left(\frac{\pi}{2}M\epsilon\right)}{M\frac{\pi}{2}\epsilon} \right|,$$

where we have considered a small offset $\epsilon \approx 0$ for the approximation [29]. Under this approach we compute the value of ϵ which provides the desired accuracy, i.e., $\sin(0.18\pi)/(0.18\pi) \approx 0.95$, leading to $\epsilon = \pm \frac{2}{M}0.18$. Next, we can exploit the geometrical relationship between the user angle θ and the module angle θ_n , as follows

$$\sin(\theta_n) = \frac{r \sin(\theta) - nSd}{r_n} = \sin(\theta) + \frac{-nSd - \Delta r_n \sin(\theta)}{r + \Delta r_n}$$

where $\Delta r_n = r_n - r$. For the sake of notation simplicity, we assume that $\sin(\theta) > 0$ and, accordingly, the larger angular differences lie on the distant modules, that is, those with $n < 0$. Then, using the fact that $\Delta r_n > 0$ in this scenario, we have that $-nSd \leq \frac{(N-1)}{2}Sd$, $-\Delta r_n \sin(\theta) \leq 0$ and $r + \Delta r_n \geq r$, thus establish the following bound

$$\frac{-nSd - \Delta r_n \sin(\theta)}{r + \Delta r_n} \leq \frac{(N-1)Sd}{2r}. \quad (29)$$

Equating this bound to ϵ the result in (24) follows.

APPENDIX C

LOW-COMPLEXITY GRAM MATRIX INVERSION

This matrix inversion procedure exploits the iterative nature of the proposed algorithms, which successively include a new user at each step. Then, at the $(n+1)$ -th iteration of the algorithm, the composite channel matrix of (26) can be written as

$$\mathbf{H}_{\bar{k}}^{(n+1)} = \begin{bmatrix} \mathbf{H}_{\bar{k}}^{(n)} \\ \mathbf{h}_{\bar{k}}^H \end{bmatrix}$$

where $\mathbf{H}_{\bar{k}}^{(n)} \in \mathbb{C}^{n \times MN}$ comprises the channels of the users selected in the $(n-1)$ former iterations, and $\mathbf{h}_{\bar{k}}$ is the channel selected at the iteration n . To compute the precoders in (26), it is necessary to obtain the Gram matrix $\mathbf{H}_{\bar{k}}^{(n+1)}(\mathbf{H}_{\bar{k}}^{(n+1)})^H$, and perform the matrix inversion

$$\mathbf{G}^{(n+1)} = \left(\mathbf{H}_{\bar{k}}^{(n+1)}(\mathbf{H}_{\bar{k}}^{(n+1)})^H \right)^{-1} \quad (30)$$

To alleviate the computational load, we propose to perform a block decomposition of the Gram matrix, leading to

$$\mathbf{G}^{(n+1)} = \left(\begin{bmatrix} \mathbf{H}_{\bar{k}}^{(n)}(\mathbf{H}_{\bar{k}}^{(n)})^H & \mathbf{H}_{\bar{k}}^{(n)}\mathbf{h}_{\bar{k}} \\ \mathbf{h}_{\bar{k}}^H(\mathbf{H}_{\bar{k}}^{(n)})^H & \|\mathbf{h}_{\bar{k}}\|^2 \end{bmatrix} \right)^{-1}.$$

Observe that the block $\mathbf{H}_{\bar{k}}^{(n)}(\mathbf{H}_{\bar{k}}^{(n)})^H$ was already included in the previous iteration of the algorithm, since $\mathbf{G}^{(n)} = (\mathbf{H}_{\bar{k}}^{(n)}(\mathbf{H}_{\bar{k}}^{(n)})^H)^{-1}$. We now apply the Schur complement to rewrite $\mathbf{G}^{(n+1)}$ as follows [30]

$$\mathbf{G}^{(n+1)} = \nu \begin{bmatrix} \frac{1}{\nu}\mathbf{G}^{(n)} + \mathbf{G}^{(n)}\xi\xi^H\mathbf{G}^{(n)} & -\mathbf{G}^{(n)}\xi \\ -\xi^H\mathbf{G}^{(n)} & 1 \end{bmatrix},$$

where we introduced the auxiliary vector $\xi = \mathbf{H}^{(n)}\mathbf{h}_{\bar{k}}$, and $\nu^{-1} = \|\mathbf{h}_{\bar{k}}\|^2 - \xi^H\mathbf{G}^{(n)}\xi$, is the Schur complement of the block $\mathbf{G}^{(n)}$ of the matrix $\mathbf{G}^{(n+1)}$. From the former equality, it is clear that the block-wise inversion only relies on the calculation of matrix-vector products. Moreover, the vector ξ and the product $\mathbf{G}^{(n)}\xi$ can be computed only once, thus reducing the computational load. According to these observations, the computational cost of obtaining $\mathbf{G}^{(n+1)}$ is in the order of $\mathcal{O}(|\mathcal{S}|MN)$, where the number of selected users $|\mathcal{S}|$ is the same as the iteration number n .

REFERENCES

- [1] O. Liberg, C. Hoymann, C. Tidestav, D. C. Larsson, I. Rahman, R. Blasco, S. Falahati, and Y. Blankenship, "Introducing 5G Advanced," *IEEE Commun. Stand. Mag.*, vol. 8, no. 1, pp. 52–57, 2024.
- [2] C.-X. Wang, X. You, X. Gao, X. Zhu, Z. Li, C. Zhang, H. Wang, Y. Huang, Y. Chen, H. Haas, J. S. Thompson, E. G. Larsson, M. D. Renzo, W. Tong, P. Zhu, X. Shen, H. V. Poor, and L. Hanzo, "On the Road to 6G: Visions, Requirements, Key Technologies, and Testbeds," *IEEE Commun. Surv. Tutor.*, vol. 25, no. 2, pp. 905–974, 2023.
- [3] B. Ning, Z. Tian, W. Mei, Z. Chen, C. Han, S. Li, J. Yuan, and R. Zhang, "Beamforming technologies for ultra-massive mimo in terahertz communications," *IEEE Open J. Commun. Soc.*, vol. 4, pp. 614–658, 2023.
- [4] M. I. Rochman, V. Sathya, N. Nunez, D. Fernandez, M. Ghosh, A. S. Ibrahim, and W. Payne, "A Comparison Study of Cellular Deployments in Chicago and Miami Using Apps on Smartphones," in *Proc. 15th ACM Workshop on Wireless Network Testbeds, Experimental Evaluation & Characterization*, ser. WiNTECH '21. New York, NY, USA: Association for Computing Machinery, 2021, p. 61–68. [Online]. Available: <https://doi.org/10.1145/3477086.3480843>
- [5] Z. Cui, P. Zhang, and S. Pollin, "6G wireless communications in 7-24 GHz band: Opportunities, techniques, and challenges," *arXiv:2310.06425*, 2023.
- [6] E. Björnson, F. Kara, N. Kolomvakis, A. Kosasih, P. Ramezani, and M. B. Salman, "Enabling 6G Performance in the Upper Mid-Band by Transitioning From Massive to Gigantic MIMO," *arXiv preprint arXiv:2407.05630*, 2024.
- [7] "Recommendation ITU-R M.2160-0: Framework and overall objectives of the future development of IMT for 2030 and beyond," 2023. [Online]. Available: <https://www.itu.int/rec/R-REC-M.2160/en>
- [8] S. Kang, M. Mezzavilla, S. Rangan, A. Madanayake, S. B. Venkatakrisnan, G. Hellbourg, M. Ghosh, H. Rahmani, and A. Dhananjay, "Cellular wireless networks in the upper mid-band," *IEEE Open J. Commun. Soc.*, vol. 5, pp. 2058–2075, 2024.
- [9] J. Jeon, G. Lee, A. A. Ibrahim, J. Yuan, G. Xu, J. Cho, E. Onggosanusi, Y. Kim, J. Lee, and J. C. Zhang, "MIMO Evolution toward 6G: Modular Massive MIMO in Low-Frequency Bands," *IEEE Commun. Mag.*, vol. 59, no. 11, pp. 52–58, Nov. 2021.
- [10] X. Li, H. Lu, Y. Zeng, S. Jin, and R. Zhang, "Near-Field Modeling and Performance Analysis of Modular Extremely Large-Scale Array Communications," *IEEE Commun. Lett.*, vol. 26, no. 7, pp. 1529–1533, Jul. 2022.
- [11] X. Li, H. Min, Y. Zeng, S. Jin, L. Dai, Y. Yuan, and R. Zhang, "Sparse MIMO for ISAC: New Opportunities and Challenges," *arXiv preprint arXiv:2406.12270*, 2024.
- [12] X. Li, Z. Dong, Y. Zeng, S. Jin, and R. Zhang, "Multi-User Modular XL-MIMO Communications: Near-Field Beam Focusing Pattern and User Grouping," *arXiv*, Aug. 2023. [Online]. Available: <https://arxiv.org/abs/2308.11289>
- [13] C. Guthy, W. Utschick, and G. Dietl, "Low-Complexity Linear Zero-Forcing for the MIMO Broadcast Channel," *IEEE J. Sel. Topics Signal Process.*, vol. 3, no. 6, pp. 1106–1117, Jan. 2009.
- [14] A. Kosasih, Ö. T. Demir, N. Kolomvakis, and E. Björnson, "The roles of spatial frequencies and degrees-of-freedom in near-field communications," *arXiv preprint arXiv:2407.07448*, 2024.
- [15] J. P. González-Coma, F. J. López-Martínez, and L. Castedo, "Low-Complexity Distance-Based Scheduling for Multi-User XL-MIMO Systems," *IEEE Wireless Commun. Lett.*, vol. 10, pp. 2407–2411, Aug. 2021.
- [16] J. H. I. de Souza, J. C. M. Filho, A. Amiri, and T. Abrão, "QoS-Aware User Scheduling in Crowded XL-MIMO Systems Under Non-Stationary Multi-State LoS/NLoS Channels," *IEEE Trans. Veh. Technol.*, vol. 72, no. 6, pp. 7639–7652, 2023.

- [17] G. J. Anaya-López, J. P. González-Coma, and F. J. López-Martínez, "Leakage Subspace Precoding and Scheduling for Physical Layer Security in Multi-User XL-MIMO Systems," *IEEE Commun. Lett.*, vol. 27, no. 2, pp. 467–471, 2023.
- [18] Z. Zhou, X. Gao, J. Fang, and Z. Chen, "Spherical Wave Channel and Analysis for Large Linear Array in LoS Conditions," *2015 IEEE Globecom Workshops (GC Wkshps)*, Dec. 2015.
- [19] E. Björnson, O. T. Demir, and L. Sanguinetti, "A Primer on Near-Field Beamforming for Arrays and Reconfigurable Intelligent Surfaces," *2021 55th Asilomar Conference on Signals, Systems, and Computers*, Oct. 2021.
- [20] M. Abramowitz and I. Stegun, *Handbook of Mathematical Functions for Scientists and Engineers (IEEE)*, ser. Applied mathematics series. Institute of Electrical and EleDover Publications, 1965.
- [21] J. Sherman, "Properties of focused apertures in the Fresnel region," *IRE Trans. Antennas Propag.*, vol. 10, no. 4, pp. 399–408, Jul. 1962.
- [22] M. Cui and L. Dai, "Channel Estimation for Extremely Large-Scale MIMO: Far-Field or Near-Field?" *IEEE Trans. Commun.*, vol. 70, no. 4, pp. 2663–2677, Apr. 2022.
- [23] X. Li, Z. Dong, Y. Zeng, S. Jin, and R. Zhang, "Multi-User Modular XL-MIMO Communications: Near-Field Beam Focusing Pattern and User Grouping," *IEEE Trans. Wireless Commun.*, pp. 1–1, 2024.
- [24] A. Kammoun, A. Müller, E. Björnson, and M. Debbah, "Linear precoding based on polynomial expansion: Large-scale multi-cell mimo systems," *IEEE J. Sel. Topics Signal Process.*, vol. 8, no. 5, pp. 861–875, 2014.
- [25] A. Benzin, G. Caire, Y. Shadmi, and A. M. Tulino, "Low-Complexity Truncated Polynomial Expansion DL Precoders and UL Receivers for Massive MIMO in Correlated Channels," *IEEE Trans. Wireless Commun.*, vol. 18, no. 2, pp. 1069–1084, 2019.
- [26] Report ITU-R M.[IMT-2020.EVAL], "Guidelines for evaluation of radio interface technologies for IMT-2020," Oct. 2017. [Online]. Available: <https://www.itu.int/md/R15-SG05-C-0057>
- [27] F. J. Martín-Vega, G. Gómez, D. Morales-Jiménez, F. J. López-Martínez, and M. C. Aguayo-Torres, "Joint Distribution of Distance and Angles in Finite Wireless Networks," *IEEE Trans. Veh. Technol.*, vol. 72, no. 10, pp. 13 281–13 297, 2023.
- [28] H. Lu and Y. Zeng, "How Does Performance Scale with Antenna Number for Extremely Large-Scale MIMO?" in *ICC 2021 - IEEE International Conference on Communications*. IEEE, Jun. 2021.
- [29] E. Björnson, C.-B. Chae, R. W. Heath, T. L. Marzetta, A. Mezghani, L. Sanguinetti, F. Rusek, M. R. Castellanos, D. Jun, and O. T. Demir, "Towards 6G MIMO: Massive Spatial Multiplexing, Dense Arrays, and Interplay Between Electromagnetics and Processing," *arXiv*, Jan. 2024.
- [30] D. Bernstein, *Matrix Mathematics: Theory, Facts, and Formulas with Application to Linear Systems Theory*. Princeton University Press, 2005.